Quantum Mechanical Rippling of a MoS_2 Monolayer Controlled by Interlayer Bilayer Coupling

Yi Zheng,[1,2] Jianyi Chen,[1] M.-F. Ng,[3] Hai Xu,[1] Yan Peng Liu,[1] Ang Li,[4] Sean J. O'Shea,[5] T. Dumitrică,[6] and Kian Ping Loh[1,2,*]

[1]*Department of Chemistry, National University of Singapore, 3 Science Drive 3, Singapore 117543*
[2]*Graphene Research Center, 6 Science Drive 2, National University of Singapore, Singapore 117546*
[3]*Institute of High Performance Computing, Agency for Science, Technology and Research, 1 Fusionopolis Way, No. 16-16 Helios, Singapore 138632*
[4]*Bruker Singapore, 11 Biopolis Way, No. 10-10 Helios, Singapore 138667*
[5]*Institute of Materials Research and Engineering, Agency for Science, Technology and Research, 3 Research Link, Singapore 117602*
[6]*Department of Mechanical Engineering, University of Minnesota, Minneapolis, Minnesota 55455,USA*

(Received 30 August 2014; published 10 February 2015)

Nanoscale corrugations are of great importance in determining the physical properties of two-dimensional crystals. However, the mechanical behavior of atomically thin films under strain is not fully understood. In this Letter, we show a layer-dependent mechanical response of molybdenum disulfide (MoS_2) subject to atomistic-precision strain induced by 2*H*-bilayer island epitaxy. Dimensional crossover in the mechanical properties is evidenced by the formation of star-shaped nanoripple arrays in the first monolayer, while rippling instability is completely suppressed in the bilayer. Microscopic-level quantum mechanical simulations reveal that the nanoscale rippling is realized by the twisting of neighboring Mo—S bonds without modifying the chemical bond length, and thus invalidates the classical continuum mechanics. The formation of nanoripple arrays significantly changes the electronic and nanotribological properties of monolayer MoS_2. Our results suggest that quantum mechanical behavior is not unique for sp^2 bonding but general for atomic membranes under strain.

DOI: 10.1103/PhysRevLett.114.065501 PACS numbers: 62.25.−g, 62.23.Kn

The physical properties of two-dimensional (2D) crystals are closely related to the atomic layer numbers, as interlayer coupling drives the dimensional crossover from 2D to bulk physics when the thickness increases discretely. Interlayer coupling leads to the striking transitions in quantum phenomena, from the massless Dirac fermions in monolayer (ML) graphene [1,2] to the massive chiral fermions in bilayer graphene [3]. In molybdenum disulfide (MoS_2), interlayer coupling is responsible for the crossover from a direct band gap semiconductor in the ML to an indirect band gap material in the bulk [4]. However, the influence of interlayer coupling on the mechanical behaviors of atomically thin 2D crystals remains less understood. Particularly, ML graphene and MoS_2 show extremely small bending rigidity κ [5–7] and exceptionally high Young's modulus E [8,9]. Such a coexistence of extreme out-of-plane flexibility and in-plane stiffness is quite unusual, considering that classical elasticity theory correlates E and κ by the relation $\kappa = [Eh_e^3/12(1-\nu^2)]$, in which h_e and ν are the elastic thickness and the Poisson ratio, respectively [10]. In the 2D limit, this continuum plate model has been challenged by theory [11] and experiment [12]. The observed subnanometer-scale rippling of graphene [12] originates in the decoupling of the bending and tensional deformations and hence invalidates the above relation. Bao *et al.* reported that at variance submicrometer ripple texture formation in suspended few-layer graphene follows the classical elasticity theory [13]. To understand elasticity in the 2D limit, the layer-dependent mechanical response of 2D crystals to strain must be studied. More importantly, as the decoupling of the bending and tensional deformations in graphene is unique for sp^2 hybridization, it is interesting to investigate whether nonclassical rippling phenomena are valid for other 2D-crystal MLs, such as in transitional metal dichalcogenides.

In this Letter, we use centrosymmetric triangular-shaped MoS_2 epilayers as a model system to study the layer-dependent mechanical properties of 2D crystals. The centrosymmetric bilayer (BL) island epitaxy on the first ML induces an atomistic-precision biaxial strain at the ML-BL boundaries by the interlayer edge-to-basal plane coupling. With the 2*H* stacking symmetry, we observe star-shaped strain patterns of one-dimensional nanoripple arrays (1D NRAs) in the ML, in contrast to the nonrippling BL island. We show that such nanoscale rippling phenomena violate the classical continuum mechanics, and its origin can be traced to the quantum-mechanical behavior of 2D-crystal MLs. The formation of nanoripple arrays effectively modifies the physical properties of ML MoS_2, affording new strategies in electronic, strain, and friction engineering in ML transitional metal dichalcogenides.

The detailed chemical vapor growth of centrosymmetric MoS_2 epilayers is described in the Supplemental Material [14]. Here, centrosymmetric growth is used to denote the growth of a second atomic-layer island on top of the first ML, both sharing the same nucleation center. Strain pattern formation in MoS_2 epilayers with the two distinct stacking symmetries of $2H$ and $3R$ [26] has been characterized by multiple atomic force microscopy techniques, Raman scattering and photoluminescence (PL).

In Figure 1(a), friction force microscopy (FFM) highlights the characteristic threefold strain patterns of 1D NRAs in the MoS_2 ML induced by $2H$ BL island growth. Dimensional crossover in the mechanical properties from the first ML to the BL can be clearly seen, as rippling instability is completely suppressed in the BL. The formation of 1D NRAs is closely correlated to the sudden increase in κ from the ML to a BL MoS_2 island. For few-layer graphene, the density functional–based tight-binding (DFTB) model predicts an $N(N^2-1)$ scaling of κ with the number of layers N. For $N=1$, the bending resistance is completely determined by the quantum mechanical π-orbital misalignment, decoupled from in-plane σ-bond stretching [11]. For the non-sp^2 MoS_2 ML, consisting of three submonolayers in the sandwiched structure of S—Mo—S connected by covalent bonds [14], such a microscopic model does not apply. However, the MoS_2 ML is also known to have an extremely low κ of a few eV [8,9,27], and thus the MoS_2 ML is expected to be slightly stretched on the rough SiO_2 surface. The formation of a centrosymmetric BL increases κ by at least an order of magnitude, even within the framework of the classical theory. The abrupt change in κ at the interface between the ML and BL created a restoring force on the stretched lattices, exerted by the more rigid bilayer [14]. Consequently, a threefold biaxial strain was created in the first ML, which was stretched along the angle-bisector directions and compressed along the ML-BL boundaries. Poisson instability induced by the compressive strain leads to out-of-plane rippling [10], which propagates along the tensile strain direction to form 1D NRAs [28]. Because of the inner symmetry of $2H$ stacking, 1D NRA formation is three folded along each angle-bisector direction to form a star-shaped strain pattern [Fig. 1(a)].

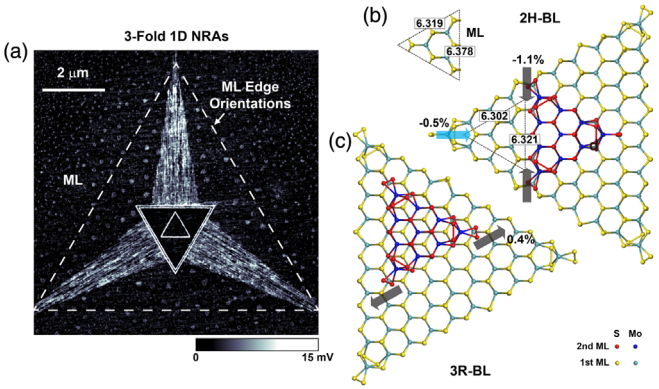

FIG. 1 (color online). Atomistic origin of 1D NRAs in MoS_2 ML induced by centrosymmetric $2H$-BL growth. (a) Characteristic FFM image of 1D NRAs in MoS_2 ML. Normal force setpoint: 1 nN. (b),(c) DFT simulation of $2H$-BL and $3R$-BL growth on a fully relaxed ML, respectively. The $2H$ BL induces compressive strain at the ML-BL boundaries, in contrast to tensile strain by the $3R$ BL. Lattice changes are in Å.

The strength of such a biaxial strain can be estimated by first principle density functional theory (DFT) calculations [14]. In Fig. 1(b), we simulated centrosymmetric $2H$-MoS_2 bilayer growth on a fully relaxed ML consisting of 227 atoms. We found that the interlayer coupling induces ~1.1% compressive strain in the vicinity of ML-BL boundaries, and ~0.5% tensile strain along the angle-bisector directions. Microscopically, the compressive strain originates from the competition between interlayer Coulomb attraction between S and Mo atoms and Pauli repulsion between S atoms at the ML-BL boundaries. In $2H$ MoS_2, the interlayer nearest-neighbor S-S repulsion force is perpendicular to the boundaries. Along the edge direction, interlayer coupling is dominated by S-Mo Coulomb interaction [14]. The bottom ML responds to the shearing Coulomb attraction by twisting the Mo—S bond, creating the compressive strain (see the quantum mechanical simulation below) [29].

Intriguingly, 1D NRAs are absent in $3R$-MoS_2 crystals. Our DFT simulation reveals that centrosymmetric $3R$-bilayer growth induces ~0.4% tensile strain along the ML-BL boundaries [Fig. 1(c)]. The transition from compressive strain in $2H$ MoS_2 to tensile strain in $3R$ MoS_2 explains the absence of 1D NRAs in the latter, since compressive strain is essential for rippling phenomena [28]. The tensile strain originates in the edge structure of the $3R$ BL, in which the interlayer nearest-neighbor S atoms are arranged in a zigzag pattern [14]. Furthermore, in $3R$ MoS_2, Mo atoms are in the hollow sites of the first ML. Such an arrangement also enhances the tensile strain by S-Mo attraction. The dominance of the Pauli repulsion force along the $3R$-MoS_2 interlayer edges is manifested by the interlayer nearest-neighbor S-S distance, which is ~0.1 Å longer than in $2H$ MoS_2 [14]. Detailed in-plane and interplane lattice changes for $2H$- and $3R$-BL growth can be found in the Supplemental Material [14].

The physical existence of 1D NRAs was also confirmed by amplitude-modulation noncontact AFM (NCAFM) and force-modulation AFM (FMAFM). The former utilizes attractive forces and does not exert compressive force on nanoripples [14], and the latter was applied to study the morphology changes of nanoripples as a function of peak tapping force. Using a peak force of 50 pN, the tip-surface interaction was minimized and the intrinsic surface morphology of 1D NRAs was imaged [Figs. 2(a) and 2(b)]. By increasing the setting to 500 pN, nanoripples become noticeably blurred due to ripple deformation under increased tip compression [Fig. 2(c)]. Further increasing the peak tapping force gradually made the 1D NRAs

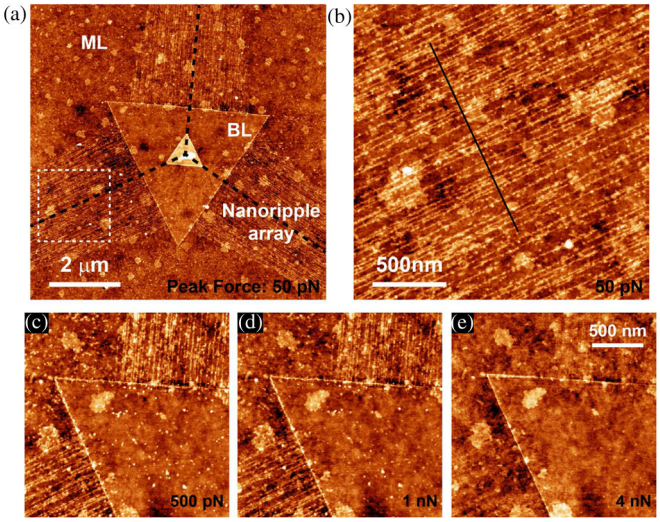

FIG. 2 (color online). Peak force-dependent FMAFM of 1D NRAs. (a) Star-shaped 1D NRAs formed along the three angle-bisector directions (indicated by the black dashed lines) of the ML due to the 2*H*-BL growth. (b) Zoom in over the dashed square in (a). The black line is the position for the cross section in Fig. 3(a). (c)–(e) Nanoripple morphology at 500 pN, 1 nN, and 4 nN peak force, respectively. Color scale: 0–2.4 nm for (a) and (b), and 0–2 nm for (c)–(e) from black to white.

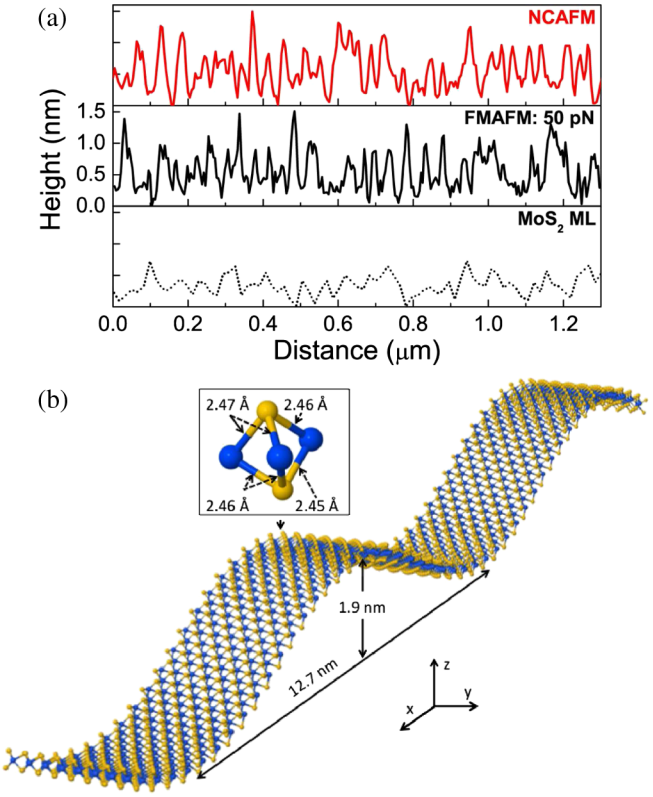

FIG. 3 (color online). Quantum mechanical simulation of 1D NRAs formation in MoS_2 ML. (a) Corrugations of 1D NRAs compared with nonrippled MoS_2 ML. (b) Atomistic simulation of a 1D NRA showing amplitude and wavelength matching the experiments. Inset shows the Mo—S bond lengths at the maximum amplitude location. The top (bottom) S atoms are located in the convex (concave) region of the ripple.

indiscernible, as shown in Figs. 2(d) (1 nN) and 2(e) (4 nN). Uniquely, FMAFM also allowed us to record the local elastic deformation at the peak-force setpoint during the topographic acquisition. Using the stiffer BL as a reference, the MoS_2 ML deformed an extra 0.25 nm on average at a force load of 4 nN, while the buckled nanoripple arrays deformed 0.35 nm [14].

We determined the physical dimensions of 1D NRAs by FFM, NCAFM, and FMAFM with good consistency [30]. Typical cross-section profiles of 1D NRAs are shown in Fig. 3(a) (the solid red and black lines), with an average nanoripple amplitude of $A \sim 1$ nm, in contrast to the featureless nonrippled MoS_2 ML (the dashed black line). The nanoripple amplitude is relatively constant over the entire strained area and is independent of the dimension of the 2*H* BL. However, the presence of a rigid substrate induces a perturbation to the periodicity of the 1D NRAs, as revealed by fast Fourier transformed topographic images. The FFT of Fig. 2(b) shows two main sets of periodicity, multiples of 23 and 26 nm [14]. Each peak is significantly broadened and has satellite peaks. Nevertheless, the basic periodicity of 1D NRAs obtained from different 2*H* crystals using FFM, NCAFM, and FMAFM converges in the range of 21–26 nm, which cannot be explained by MoS_2-substrate coupling, considering the amorphous nature of SiO_2. More importantly, 1D NRAs are absent in pure ML and 3*R* MoS_2, which constitute 76% of all the grown crystals [14]. We have also observed quadruple MoS_2 crystals stacked in 3*R*-3*R*-2*H* sequences from bottom to top. The emergence of 1D NRAs in the third ML due to 2*H* coupling with the fourth ML provides convincing evidence of the atomic origin of the interlayer edge-to-basal plane coupling [14].

We compared the 1D NRAs on MoS_2 with the experimental reports on periodic ripples in graphene. In Ref. [13], Bao *et al.* studied the formation of 1D periodical ripples in suspended graphene membranes induced by thermal treatment. Their report claims that ripple formation in atomically thin films follows the classical elasticity theory, which correlates A, the wavelength λ, and the thickness of the atomic membrane t as

$$\lambda = \frac{(2\pi L t)^{(1/2)}}{[3(1-\nu^2)\gamma]^{(1/4)}};$$
$$A = (\nu L t)^{(1/2)}\left[\frac{16\gamma}{3\pi^2(1-\nu^2)}\right]^{(1/4)}, \quad (1)$$

where L is the length of the suspended channel, and γ is the tensile strain induced by the thermal treatment. By eliminating the sample-dependent γ, the classical theory requires A, λ, and t to satisfy a constant condition:

$$\frac{A\lambda}{Lt} = \sqrt{\frac{8\nu}{3(1-\nu^2)}}. \quad (2)$$

These equations describe the micrometer-sized ripple in Ref. [13], in which λ ranges from 0.37 to 5 μm. However, the applicability of classical elasticity theory to 2D MLs has been challenged by periodic subnanometer-wavelength rippling in a suspended graphene ML grown on Cu(111) [12]. At this length scale, which is close to the lattice constant of graphene, $(A\lambda/Lt)$ is smaller than $\sqrt{[8\nu/3(1-\nu^2)]}$ by more than an order of magnitude. We found that the classical elastic theory is also violated by the physical dimensions of the 1D NRAs in $2H$-MoS_2 multilayers. Taking $A = 1$ nm, $\lambda = 23$ nm, $L = 1$ μm, $t = 0.46$ nm, and $\nu = 0.26$ [31], the relation in Eq. (2) fails by at least a factor of 10. Alternatively, we can use Eq. (2) to calculate an equivalent plate thickness to match the experimental observations. The deduced equivalent t is 0.17 Å, which is certainly unrealistic [14].

We confirmed the quantum mechanical origin of rippling in ML MoS_2 with microscopic-level simulations using DFTB [27]. A simulation domain containing 144 atoms was placed under periodic boundary conditions along the x-y in-plane directions. Compressive strain was applied by a protocol that gradually varied the periodicity along the x direction followed by conjugate gradient relaxation simulations [14]. In contrast to the classical modeling, we found that the microscopic approach can reproduce the nanometer-scale rippling observed in our AFM studies. Indeed, Fig. 3(b) shows a periodic rippling exhibited by the MoS_2 ML with a wavelength of 12.7 nm and an amplitude of 0.95 nm, in excellent agreement with the experimental measurements presented in Fig. 3(a). The analysis of the bond lengths shown in the inset offers an intuitive explanation for the violation of the plate behavior. The classical bending of a plate involves asymmetrical stretching and compression on the material located on the opposite sides of the neutral line. In contrast, the Mo—S bonds located in the concave and convex regions of the ripple are practically identical in length. This is because the S atoms are free to move along the out-of-plane direction to relax the strain in the Mo—S bonds. Thus, although in the S-Mo-S trilayer, MoS_2 can still easily curve because of its microscopic structure, which allows the twisting of neighboring Mo—S bonds without modifying the chemical bond length.

Using Raman scattering and PL, we qualitatively determined the strain type and strain intensity of the 1D NRAs. For Raman scattering [Figs. 4(a) and 4(b)], we selected twinned crystals with the concentric bilayer growth located on the right twin [14]. In Raman mapping, significant phonon hardening was observed, as manifested by blue shifts in both in-plane (E^1_{2g}) and out-of-plane (A_{1g}) vibration modes [Fig. 4(a)]. Based on the Raman shift of ~ 2 cm^{-1} for A_{1g} [Fig. 4(b)], we estimate that the corresponding average compressive strain is about 1% [32,33]. This compares favorably to the strains estimated from the DFT calculations in Fig. 1(b). The compressive nature of the strain formed in 1D NRAs is also confirmed by the narrowing of the full width at half maximum

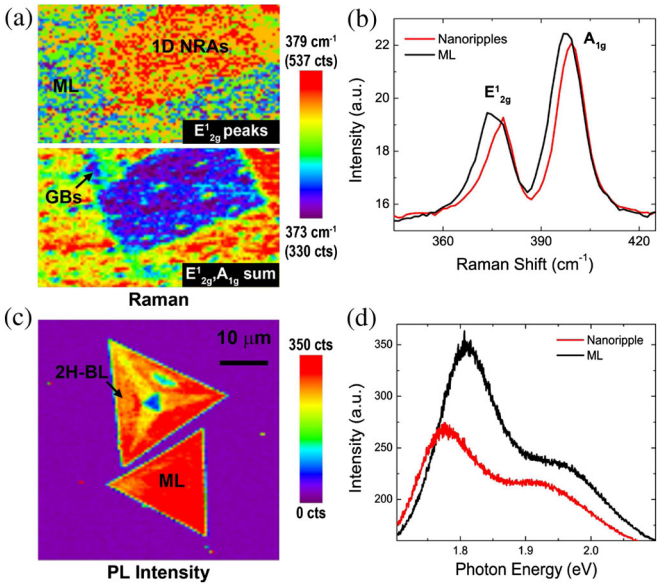

FIG. 4 (color online). (a),(b) Raman characterizations of 1D NRAs formed in twinned crystals. The average strain intensity is estimated as ~1%. (c),(d) PL measurements of 1D NRAs. The measured shift in photon energy peaks agrees with the Raman results.

(FWHM) of both the E^1_{2g} and A_{1g} peaks [Fig. 4(b)]. The estimated strain intensity agrees well with the PL experiment, which indicates an equivalent strain of ~0.7% based on a 41 meV change in PL peak positions [34] [Figs. 4(c) and 4(d)]. Therefore, both the Raman scattering and PL results support the microscopic origin of the biaxial strain from interlayer coupling, as revealed by the DFT simulation.

Our studies show that an atomistic rippling instability induced by strong interlayer edge-to-basal plane coupling causes quantum mechanical rippling phenomena in the MoS_2 ML, but does not influence the BL. Such an atomistic rippling instability is unique in its dependence on geometrical bilayer stacking and the pronounced threefold symmetry, which are fundamentally different from the previously reported nanorippling instability in 2D material, such as strain accumulation at the grain boundaries [14,35]. The results provide direct evidence of the layer-dependent mechanical properties of 2D crystals, and suggest quantum mechanical rippling that violates classical mechanics may be generic to 2D MLs. Despite the atomistic origin, 1D NRAs show robust resistance to perturbation by a rough SiO_2 substrate and can extend for tens of micrometers along the tensile strain direction. This opens the possibility for micro- or nanodevice fabrications, in which 1D NRAs are utilized as active channels. Centrosymmetric bilayer epitaxy may also provide an efficient way to form 2D van der Waals heterostructures [36] and 1D topological defects, such as solitonlike strain boundaries [37,38].

We thank Antonio Castro-Neto and Jens Martin for insightful discussions. We acknowledge funding support

from the National Research Foundation CRP grant "Plasmon Electronics, New Generation of Devices to Bypass Fundamental Limitations." The DFT simulations were supported by the A*STAR Computational Resource Centre (ACRC) in Singapore through the use of its high performance computing facilities. T. D. acknowledges funding support from NSF Grant No. 1006706.

Y. Z. and J. C. contributed equally to this work.

*chmlohkp@nus.edu.sg

[1] K. S. Novoselov, A. K. Geim, S. V. Morozov, D. Jiang, M. I. Katsnelson, I. V. Grigorieva, S. V. Dubonos, and A. A. Firsov, Nature (London) **438**, 197 (2005).

[2] Y. Zhang, Y. W. Tan, H. L. Stormer, and P. Kim, Nature (London) **438**, 201 (2005).

[3] K. S. Novoselov, E. Mccann, S. V. Morozov, V. I. Fal'ko, M. I. Katsnelson, U. Zeitler, D. Jiang, F. Schedin, and A. K. Geim, Nat. Phys. **2**, 177 (2006).

[4] K. F. Mak, C. Lee, J. Hone, J. Shan, and T. F. Heinz, Phys. Rev. Lett. **105**, 136805 (2010).

[5] C. Lee, X. Wei, J. W. Kysar, and J. Hone, Science **321**, 385 (2008).

[6] P. Johari and V. B. Shenoy, ACS Nano **6**, 5449 (2012).

[7] A. Castellanos-Gomez, M. Poot, G. A. Steele, H. S. J. van der Zant, N. Agrait, and G. Rubio-Bollinger, Adv. Mater. **24**, 772 (2012).

[8] Y. Wei, B. Wang, J. Wu, R. Yang, and M. L. Dunn, Nano Lett. **13**, 26 (2013).

[9] N. Lindahl, D. Midtvedt, J. Svensson, O. L. Nerushev, N. Lindvall, A. Isacsson, and E. E. B. Campbell, Nano Lett. **12**, 3526 (2012).

[10] L. D. Landau and E. M. Lifshitz, *Theory of Elasticity* (Pergamon Press, New York, 1970).

[11] D. B. Zhang, E. Akatyeva, and T. Dumitrică, Phys. Rev. Lett. **106**, 255503 (2011).

[12] L. Tapaszto, T. Dumitrica, S. J. Kim, P. Nemes-Incze, C. Hwang, and L. P. Biro, Nat. Phys. **8**, 739 (2012).

[13] W. Bao, F. Miao, Z. Chen, H. Zhang, W. Jang, C. Dames, and C. N. Lau, Nat. Nanotechnol. **4**, 562 (2009).

[14] See Supplemental Material at http://link.aps.org/supplemental/10.1103/PhysRevLett.114.065501, which includes Ref. [15–25], for CVD growth and DFT calculations.

[15] I. Horcas, R. Fernández, J. M. Gómez-Rodriguez, J. Colchero, J. Gómez-Herrero, and A. M. Baro, Rev. Sci. Instrum. **78**, 013705 (2007).

[16] B. B. Pittenger, N. Erina, and C. Su, *Quantitative Mechanical Property Mapping at the Nanoscale with PeakForce QNM* (Bruker, Santa Barbara, CA, 2012), http://www.bruker.com/fileadmin/user_upload/8-PDF-Docs/SurfaceAnalysis/AFM/ApplicationNotes/AN128-RevB0-Quantitative_Mechanical_Property_Mapping_at_the_Nanoscale_with_PeakForceQNM-AppNote.pdf.

[17] J. P. Perdew, K. Burke, and M. Ernzerhof, Phys. Rev. Lett. **77**, 3865 (1996).

[18] S. Grimme, J. Comput. Chem. **27**, 1787 (2006).

[19] G. Kresse and J. Furthmüller, Comput. Mater. Sci. **6**, 15 (1996).

[20] G. Kresse and J. Furthmüller, Phys. Rev. B **54**, 11169 (1996).

[21] P. E. Blöchl, Phys. Rev. B **50**, 17953 (1994).

[22] A. Socoliuc, E. Gnecco, S. Maier, O. Pfeiffer, A. Baratoff, R. Bennewitz, and E. Meyer, Science **313**, 207 (2006).

[23] M. Dienwiebel, G. S. Verhoeven, N. Pradeep, J. W. M. Frenken, J. A. Heimberg, and H. W. Zandbergen, Phys. Rev. Lett. **92**, 126101 (2004).

[24] X. S. Li, W. Cai, J. An, S. Kim, J. Nah, D. Yang, R. Piner, A. Velamakanni, I. Jung, E. Tutuc, S. K. Banerjee, L. Colombo, and R. S. Ruoff, Science **324**, 1312 (2009).

[25] G. X. Ni, Y. Zheng, S. Bae, H. R. Kim, A. Pachoud, Y. S. Kim, C. L. Tan, D. Im, J. H. Ahn, B. H. Hong, and B. Özyilmaz, ACS Nano **6**, 1158 (2012).

[26] H. Bergmann, B. Czeska, I. Haas, B. Mohsin, and K. H. Wandner, *Gmelin Handbook of Inorganic and Organometallic Chemistry* (Springer-Verlag, Berlin, 1992).

[27] D. B. Zhang, T. Dumitrică, and G. Seifert, Phys. Rev. Lett. **104**, 065502 (2010).

[28] E. Cerda and L. Mahadevan, Phys. Rev. Lett. **90**, 074302 (2003).

[29] It is noteworthy that the biaxial strain is underestimated in the DFT simulation because the effects of substrate roughness are excluded from the calculation. Furthermore, the MoS_2 epilayer had a much larger thermal expansion coefficient than the SiO_2 substrate [see J. Appl. Crystallogr. **9**, 403 (1976)]. During crystal growth, there was a significant tensile strain buildup, which was pinned by **MoS_2**-substrate interactions.

[30] 1D NRAs are not visible in the contact AFM (CAFM) topographic images, indicating that there is substantial elastic deformation of nanoripples in the contact mode. In contrast, FFM was enhanced by the localized compression and deformation of 1D NRAs when the tip was moving across the rippled textures. The dominant friction interaction between the 2D-cyrstal ML and the CAFM tip has been reported previously, showing that kinetic friction is increased by a factor of 2 to 3 due to the out-of-plane deformation of atomically thin films [see Science **328**, 76 (2010)]. Here, by forming 1D NRAs, kinetic friction was further increased by about 2 times, mainly due to the large elastic deformation of the nanoripples.

[31] J. L. Feldman, J. Phys. Chem. Solids **37**, 1141 (1976).

[32] K. He, C. Poole, K. F. Mak, and J. Shan, Nano Lett. **13**, 2931 (2013).

[33] Y. Y. Hui, X. Liu, W. Jie, N. Y. Chan, J. Hao, Y. Hsu, L. Li, W. Gao, and S. P. Lau, ACS Nano **7**, 7126 (2013).

[34] H. J. Conley, B. Wang, J. I. Ziegler, R. F. Haglund, Jr., S. T. Pantelides, and K. I. Bolotin, Nano Lett. **13**, 3626 (2013).

[35] P. Yeh, W. Jin, N. Zaki *et al.*, Phys. Rev. B **89**, 155408 (2014).

[36] A. K. Geim and I. V. Grigorieva, Nature (London) **499**, 419 (2013).

[37] C. R. Woods *et al.*, Nat. Phys. **10**, 451 (2014).

[38] J. S. Alden, A. W. Tsen, P. Y. Huang, R. Hovden, L. Brown, J. Park, D. A. Muller, and P. L. McEuen, Proc. Natl. Acad. Sci. U.S.A. **110**, 11256 (2013).